arXiv:nucl-th/0612094v1 20 Dec 2006

Superdeformation and hyperdeformation in the ^{108}Cd nucleus.

A. V. Afanasjev$^{(1,2)}$, S. Frauendorf$^{(1,3)}$
^{1}*Department of Physics, University of Notre Dame, Notre Dame, Indiana 46556, USA*
^{2} *Department of Physics and Astronomy, Mississippi State University, MS 39762, USA and*
^{3}*IKH, Research Center Rossendorf, Dresden, Germany*
(Dated: February 9, 2008)

The superdeformation and hyperdeformation in ^{108}Cd have been studied for the first time within the framework of the fully self-consistent cranked mean field theory, namely, cranked relativistic mean field theory. The structure of observed superdeformed bands 1 and 2 have been analyzed in detail. The bumps seen in their dynamic moments of inertia are explained as arising from unpaired band crossings. This is contrary to an explanation given earlier within the framework of projected shell model. It was also concluded that this nucleus is not doubly magic SD nucleus.

PACS numbers: 21.60.Jz, 21.60.Cs, 27.60.+j

Since the discovery of superdeformation in ^{152}Dy two decades ago [1], nuclear super- and hyperdeformation have been in the focus of attention of nuclear structure community. At present, superdeformation (SD) has been discovered in different mass regions and extensively studied experimentally [2] and theoretically (see, for example, Ref. [3] and references therein). On the other side, nothing is known experimentally about hyperdeformation (HD) apart from some indications of this phenomenon at low spin in the uranium nuclei [4].

Recent observation of the very extended shapes in ^{108}Cd [5, 6] has opened new region of superdeformation and renewed interest to the study of hyperdeformation [7]. Two SD bands have been found in this nucleus. In the present manuscript, they are labeled according to Ref. [6], namely, the lowest SD band as band 1 and the excited SD band as band 2. These experiments were strongly motivated by earlier calculations of Ref. [8] and more recent studies of Ref. [9].

So far theoretical interpretation has been performed only for band 1 within the framework of projected shell model (PSM) (Ref. [10]). Clear deficiency of this description is the fact that the equilibrium deformation is not defined within some "variational" procedure, but is adjusted for a better description of moments of inertia. It was concluded in Ref. [10] that the low-K $i_{13/2}$ proton orbitals are responsible for the observed bump in the dynamic moment of inertia $J^{(2)}$ at low rotational frequencies and that the 2-quasiparticle configurations from these orbitals dominate the structure of the observed states. However, it is well known that the pairing is considerably quenched at high rotational frequencies and superdeformation [11, 12]. For example, no paired band crossing is observed above rotational frequencies $\omega \sim 0.5$ MeV in the $A \sim 150$ [3, 13, 14] and $\omega \sim 1.0$ MeV in the $A \sim 60$ [14, 15] mass regions of superdeformation and the experimental data above these frequencies are well (within $\approx 5\%$ accuracy for the moments of inertia) described by the cranked relativistic mean field (CRMF) theory with no pairing. Considering that the $A \sim 110$ mass region of superdeformation is located between these two regions, it is reasonable to expect that the influence of pairing will be negligible above $\omega \geq 0.8 - 0.9$ MeV. Thus, rephrasing the results of the PSM studies in Ref. [10] to the language of the calculations without pairing, one can conclude that the $\pi 6^2$ configuration has to be assigned to the band 1 in ^{108}Cd above the band crossing. The $\pi 6^2$ SD configurations are active in the medium-mass part of the rare-earth region of superdeformation [Gd ($Z = 64$) nuclei] [3]. However, the Fermi level is located at much lower $Z = 48$ in ^{108}Cd as compared with the $A \sim 150$ mass region of superdeformation, and, thus, considerably larger deformation and higher rotational frequencies than in the rare-earth region of SD will be required to have the two lowest $N = 6$ proton orbitals occupied.

In the present manuscript, the CRMF theory [3, 16] is used for detailed investigation of the structure of observed SD bands in ^{108}Cd and the nature of hyperdeformation in the $A \sim 110$ mass region. Additional insight has been provided by the cranked Nilsson-Strutinsky (CNS [12]) calculations performed with the standard Nilsson parameters [17]. In both calculations, the pairing is neglected. The CRMF equations are solved in the basis of an anisotropic three-dimensional harmonic oscillator in Cartesian coordinates with the deformation parameters $\beta_0 = 0.65$, $\gamma = 0°$ and oscillator frequency $\hbar\omega_0 = 41A^{-1/3}$ MeV. All fermionic and bosonic states belonging to the shells up to $N_F = 14$ and $N_B = 16$ are taken into account in the diagonalization of the Dirac equation and the matrix inversion of the Klein-Gordon equations, respectively. The detailed investigation indicates that this truncation scheme provides good numerical accuracy. The NL1 set [18] is used for the RMF Lagrangian. As follows from our experience [13, 19], this set provides reasonable description of the single-particle energies.

The results of the CRMF calculations for the configurations forming the yrast line or located close to it in energy are shown in Fig. 1. According to these calculations, normal-deformed bands, many of which show high triaxiality indicative of approaching band termination, dominate the yrast line up to $I \approx 68\hbar$. At higher spin hyperdeformed bands become yrast. The SD bands are never yrast, but come close to the yrast line at $I \approx 66\hbar$.

The lowest SD configuration has $(\pi = +, r = +1)$ (even spins) quantum numbers and it is assigned to band 1. We assign bands 1 and 2 to SD configurations, because the calculated kinematic $J^{(1)}$ and dynamic $J^{(2)}$ moments of inertia agree well with experiment. The configurations with normal deformation have too small and the configurations with hyperdeformation too large values of moments of inertia. The experimental values of transition quadrupole moment Q_t are best reproduced by the SD configurations. The proton and neutron single-routhian diagrams along the deformation path of this configuration are shown in Fig. 2. Before unpaired band crossing it has the $\pi 6^0 \nu 6^2$ structure, while after band crossing the $\pi 6^1 \nu 6^2$ structure. The unpaired band crossing is due to the crossing of the $\pi[420]1/2(r = -i)$ and $\pi[660]1/2(r = -i)$ orbitals (arrow A in Fig. 2). The exact band crossing frequencies are not known for bands 1 and 2 because downsloping branches of $J^{(2)}$ below the band crossing have not been observed. The comparison of the experimental and calculated bumps in $J^{(2)}$ suggests that the crossing takes place ≈ 200 keV earlier in the calculations than in experiment (see Fig. 3). The frequency of this band crossing depends on the relative position of the above mentioned orbitals and thus the discrepancy between experiment and theory suggests that the relative energy distance between these orbitals is underestimated in the calculations by approximately 0.7 MeV. The CRMF calculations well reproduce the absolute value of dynamic moment of inertia $J^{(2)}$ above the band crossing, but underestimate somewhat the height of the bump in dynamic moment of inertia $J^{(2)}$ at the band crossing (Fig. 3b).

The best agreement between calculated and 'experimental' kinematic moments of inertia $J^{(1)}$ is seen if the lowest state in band 1 has spin $I_0 = 44\hbar$ (Fig. 3a). This suggests that the band in ^{108}Cd has been observed in the spin range from $44\hbar$ up to $66\hbar$. However, taking into account that typical accuracy of the description of the moments of inertia in the CRMF calculations is around 5% [3, 14, 15] and possible minor impact of pairing at high rotational frequencies, which would lead to slight decrease of calculated $J^{(1)}$ [14], one cannot completely exclude that the lowest SD band in ^{108}Cd has been observed from $42\hbar$ up to $64\hbar$. The spin range $I = 40(2) - 60(2)\hbar$ has been suggested in Ref. [5] using the assumption that $J^{(1)} \simeq J^{(2)}$. However, this assumption is not supported by our calculations where $J^{(2)} \approx 0.88 J^{(1)}$ for assigned configuration above the band crossing.

The average transition quadrupole moment of the assigned configuration in the suggested spin range is $Q_t \approx 10.8$ eb, which agrees with the lower limit of $Q_t = 9.5$ eb obtained in experiment [5]. The occupation of the first proton $N = 6$ orbital at the band crossing has only minor impact on Q_t: an increase of Q_t by approximately 0.2 eb.

Band 2 has the features similar to the band 1 except that the band crossing takes place ≈ 200 keV earlier (Fig. 3b). Especially interesting is the observation that the $J^{(2)}$ moments of inertia of these two bands are very similar above the band crossing. Similar to the $A \sim 150$ region of superdeformation [3, 21], this suggests that the intruder content of observed bands should be the same. The only possible explanation found in our calculations is related to the excitation of proton from the $\pi[420]1/2(r = +i)$ orbital into the lowest positive parity orbital with signature $r = -i$ above the $Z = 48$ shell gap (see Fig. 2). In Fig. 2 above $\omega = 0.2$ MeV, this orbital has the $\pi[422]3/2$ structure. However, contrary to the situation shown in Fig. 2 at equilibrium deformation of the configuration of interest the $[422]3/2(r = \pm i)$ orbitals are located below the $\pi[413]7/2(r = \pm i)$ orbitals even at zero rotational frequency. At $\omega \approx 0.35$ MeV, the $\pi[422]3/2(r = -i)$ and the $\pi[660]1/2(r = -i)$ orbitals interact strongly. This interaction creates the bump in $J^{(2)}$ (Fig. 3b). Above the band crossing, the calculated $J^{(2)}$ reproduces well the experimental one and is very close to the $J^{(2)}$ values of the configuration assigned to the lowest SD band, the feature observed also in experiment.

When interpreting band 2, we also considered particle-hole excitations in neutron subsystem, namely from the $\nu[660]1/2(r = +i)$ orbital to the $\nu[303]5/2(r = \pm i)$ orbitals (Fig. 2). Such excitations lead to smaller deformation, and thus to the delay of the unpaired band crossing (originating from interaction of the $\pi[420]1/2(r = +i)$ and the $\pi[660]1/2(r = +i)$ orbitals). For example, in the configuration based on the occupied $\nu[303]5/2(r = -i)$ orbital this crossing is delayed by ≈ 0.35 MeV, which is in contradiction with experiment.

Therefore, similar to the configuration assigned to the band 1, the structure of the configuration assigned to the band 2 changes from $\pi 6^0 \nu 6^2$ to $\pi 6^1 \nu 6^2$ at the band crossing. However, it has total signature $r = -1$ (odd spins) and negative parity. The band crossing A, active in the configuration of the band 1, is not active in the configuration of band 2 since both interacting orbitals ($\pi[420]1/2(r = -i)$ and $\pi[660]1/2(r = -i)$) are occupied (see Fig. 2). Since the $\pi[413]7/2(r = -i)$ and $\pi[660]1/2(r = -i)$ orbitals interact very weakly (see inside of ellipse B in Fig. 2), their interaction cannot explain the observed features of band 2 in the band crossing region. The comparison of relative alignments of bands 2 and 1 (Fig. 3) suggests that with $I_0 = 44\hbar$ assigned for initial state of band 1, the band 2 has been observed in the spin range from $I_0 = 43\hbar$ up to $I = 65\hbar$. In the region beyond band crossing ($\omega = 0.9 - 1.2$ MeV), the calculated relative alignments differ from the experimental ones only by $\approx 0.3\hbar$: this is within the typical uncertainty of the description of relative alignments in the CRMF theory [13, 15, 20].

The calculations show that the quadrupole deformations of the configurations assigned to the bands 1 and 2 are almost the same, but they differ somewhat in the γ-deformation. While the configuration of band 1 has $\gamma \approx 6°$, the one of the band 2 has $\gamma \approx -4°$. As a consequence, the configuration of the band 2 is more collective ($Q_t \approx 12.2$ eb) as compared with the one of band 1. Although the experimental analysis for band 2 yielded a lower value for the transition quadrupole moment $Q_t = 8.5$ eb, it suffered from the large errors on the $F(\tau)$ values which did not allow an accurate measurement of the Q_t values [6]. Thus based on the similarity of rotational properties of bands 1 and 2 above the band crossing and the results of the CRMF calculations, it is reasonable to believe that the deformation for band 2 is comparable to the one for band 1 (see also Ref. [6]).

The earlier band crossing in the configuration of band 2 as compared with experiment is due to small energy distance between the $\pi[422]3/2$ and $\pi[660]1/2$ orbitals in the calculations. In order to have this crossing at experimentally observed frequency, one should increase this distance by ≈ 0.7 MeV. This value is similar to the underestimate of the energy distance between the $\pi[420]1/2$ and $\pi[660]1/2$ orbitals deduced earlier. This suggests that the energy distance between the $\pi[422]3/2$ and $\pi[420]1/2$ orbitals, and, consequently the $Z = 48$ SD shell gap is reasonably well reproduced in the calculations. Thus, one concludes that the $Z = 48$ SD shell gap is smaller than the $Z = 30$ SD shell gap in the $A \sim 60$ region of superdeformation (see Fig. 1 in Ref. [15]) and $Z = 66$ SD shell gap in the rare-earth region of superdeformation (see Fig. 3 in Ref. [3]). This maybe a possible reason why the search for SD bands in neighbouring nuclei has been unsuccesful so far [22].

In addition, it indicates that in reality the $\pi[660]1/2$ orbital is located ≈ 0.7 MeV higher in energy with respect of the $\pi[420]1/2$ and $\pi[422]3/2$ orbitals than suggested by the present calculations. This is not far away from the typical accuracy with which the energies of the single-particle states are reproduced at normal- [19] and superdeformation [13] in the RMF calculations with the NL1 set.

Unpaired band crossings at superdeformation were reported earlier, for example, in ^{146,147}Gd [3, 24] and ^{153}Ho [23]. The band crossing in the SD band 1 of ^{153}Ho is similar to the ones seen in ^{108}Cd since it involves the interaction of the routhians with $\Delta N = 2$.

The hyperdeformed configurations become yrast above $I = 68\hbar$ (Fig. 1). These are the signature partner $\pi 6^2 \nu 6^4 7^1$ configurations of negative parity which are degenerated in energy. This energy degeneracy is due to the excitation of one neutron from the $\nu[413]7/2(r = \pm i)$ orbitals into the lowest $N = 7$ orbital (see Fig. 4). The HD configurations are favoured in energy at these spins due to the $Z = 48$ HD shell gap and low neutron level density at $N = 59 - 61$. The transition quadrupole moment Q_t increases from $Q_t = 17.2$ eb at $I = 44\hbar$ up to $Q_t \approx 17.5\hbar$ at $I = 84\hbar$. This fact is related to the stretching of the nucleus due to centrifugal force. The shape of nucleus corresponds to the 2.3:1 semiaxis ratio (Fig. 5). The kinematic moment of inertia drops down from $J^{(1)} \approx 70.5$ MeV^{-1} at $I = 44\hbar$ to $J^{(1)} \approx 67.5$ MeV^{-1} at $I = 84\hbar$. In the frequency range where the experimental bands 1 and 2 have been observed, the dynamic moments of inertia of calculated configurations are equal to $J^{(2)} \approx 64$ MeV^{-1}; the quantity which is much larger than in experiment. At higher frequencies there is smooth increase of $J^{(2)}$ up to ≈ 70 MeV^{-1} at $\omega \sim 1.4$ MeV, possibly caused by unpaired band interaction. No experimental counterparts of these configurations have been observed so far.

It is interesting to mention the similarity of the single-particle spectra at hyperdeformation obtained in the CRMF calculations (Fig. 4) and in the Wood-Saxon-Strutinsky calculations of Ref. [9] (Fig. 4 and 5 of Ref. [9]). However, the $N = 61$ ($N = 58$ and $N = 59$) shell gaps are somewhat smaller (larger) in the CRMF calculations. In the later calculations, the quadrupole, octupole, hexadecapole and necking degrees of freedom were taken into account. There are, however, no indications that octupole deformation should play a role at HD in ^{108}Cd [9]. On the other side, the CRMF calculations take into account all even-multipole deformations and triaxiality in a fully self-consistent way. The basis of the CRMF model is sufficiently large to see if there is a pronounced tendency for the development of necking. Fig. 5, showing the densities of lowest HD configuration, does not indicate such a tendency.

The CNS calculations, which will not be discussed here in detail, also indicate that the band 1 in ^{108}Cd is associated with the $\pi 6^1 \nu 6^2$ configuration having $Q_t \sim 10.3$ eb and located in the $\varepsilon_2 \sim 0.67, \gamma \sim 15^\circ$ minimum. Similar to earlier calculations (Ref. [15]), the triaxiality is more pronounced in the CNS calculations for ^{108}Cd as compared with the CRMF ones. In the CNS calculations, the HD configurations are yrast above $I \approx 63\hbar$, and the $\pi 6^2 \nu 6^4 7^1$ configurations with $Q_t \approx 18$ eb are the lowest ones. Thus, one can conclude that general properties of SD and HD bands are similar in both approaches.

The present CRMF calculations suggest that in the spin range where the feeding of SD bands takes place (i) the SD bands are non-yrast and (ii) the HD bands compete in energy with the SD bands. However, only SD bands have been reported at high spin in Refs. [5, 6]. Because of limited experimental information it is difficult to find unique explanation for this discrepancy. On one side, one would expect that the calculated relative energies of different minima deviate somewhat from reality. Alternative explanation is related to the differences in feeding mechanism of SD and HD bands [25]. Although the HD and SD states are comparable in energy at $I \sim 66\hbar$ at zero temperature (Fig. 1), these high spin nuclear states are populated at somewhat higher spin at temperatures $T \sim 1.0$ MeV. At these temperatures, the deformed shell structure melts, and thus SD minimum becomes lower in energy than HD one. As a consequence, the feeding of the SD minimum maybe the dominant population channel [25].

In summary, the detailed analysis of the structure of observed superdeformed bands 1 and 2 in ^{108}Cd within the cranked relativistic mean field theory led to new configuration assignment: both bands have been assigned the $\pi 6^1 \nu 6^2$ configurations. The band crossings seen in these bands have been related to the unpaired crossings of the lowest proton $N = 6$ orbital and the $N = 4$ orbitals. The size of the $Z = 48$ SD shell gap, which is smaller than that of doubly magic ^{60}Zn and ^{152}Dy SD nuclei, and the absence of large neutron shell gap at $N = 60$ indicate that the ^{108}Cd nucleus cannot be considered as a doubly magic SD nucleus. The properties of hyperdeformed configurations, which are expected to be yrast above $I \approx 64\hbar$, have also been discussed.

I. ACKNOWLEDGEMENTS

The work was supported by the DoE grant DE-F05-96ER-40983. The help of Y. Gu in performing CNS calculations and the discussions with I. Ragnarsson are highly appreciated.

[1] P. J. Twin *et al*, Phys. Rev. Lett. **57**, 811 (1986).
[2] B. Singh, R. Zywina, R. B. Firestone, Nucl. Data Sheets **97**, 241 (2002).
[3] A. V. Afanasjev, J. König and P. Ring, Nucl. Phys. **A608**, 107 (1996)
[4] A. Krasznahorkay *et al*, Phys. Rev. Lett. **80**, 2073 (1998).
[5] R. M. Clark *et al*, Phys. Rev. Lett. 87, 202502 (2001).
[6] A. Görgen *et al*, Phys. Rev. **C65**, 027302 (2002).
[7] B. M. Nyako *et al*, Acta Phys. Pol. **B36**, 1033 (2005), H. Hübel *et al*, ibid **B36**, 1015 (2005), B. Herskind, Phys. Scripta, in press
[8] T. Werner and J. Dudek, At. Data Nucl. Data Tables **59**, 1 (1995).
[9] R. R. Chasman, Phys. Rev. **C64**, 024311 (2001).
[10] C.-T. Lee, Y. Sun, Jing-ye Zhang, M. Guidry, and C.-L. Wu, Phys. Rev. **C65**, 041301(R) (2002).
[11] Y. R. Shimizu *et al*, Rev. Mod. Phys. **61**, 131 (1989).
[12] A. V. Afanasjev, D. B. Fossan, G. J. Lane and I. Ragnarsson, Phys. Rep. **322**, 1 (1999).
[13] A. V. Afanasjev, G. Lalazissis and P. Ring, Nucl. Phys. **A634**, 395 (1996).
[14] D. Vretenar, A. V. Afanasjev, G. A. Lalazissis, P. Ring, Phys. Rep. **409**, 101 (2005).
[15] A. V. Afanasjev, I. Ragnarsson and P. Ring, Phys. Rev. C **59**, 3166 (1999).
[16] W. Koepf and P. Ring, Nucl. Phys. **A493**, 61 (1989).
[17] T. Bengtsson and I. Ragnarsson, Nucl. Phys. **A436**, 14 (1985).
[18] P.-G. Reinhard *et al*, Z. Phys. **A323**, 13 (1986).
[19] A. V. Afanasjev *et al*, Phys. Rev. C **67**, 024309 (2003).
[20] A. V. Afanasjev and S. Frauendorf, Phys. Rev. C **71**, 064318 (2005).
[21] T. Bengtsson, I. Ragnarsson and S. Åberg, Phys. Lett. **B208**, 39 (1988).
[22] P. Fallon, Nucl. Phys. **A752**, 231c (2005).
[23] A. V. Afanasjev and P. Ring, Nucl. Phys. **A654**, 647c (1999).
[24] B. Haas *et al*, Nucl. Phys. **A561**, 251 (1993).
[25] J. Dudek *et al*, Eur. Phys. J **A20**, 15 (2004).

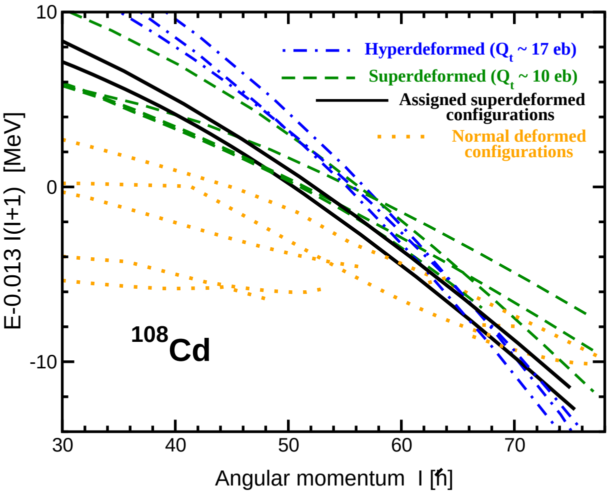

FIG. 1: Energies of the configurations calculated in the CRMF theory relative to a smooth liquid drop reference $AI(I+1)$, with the inertia parameter $A = 0.013$.

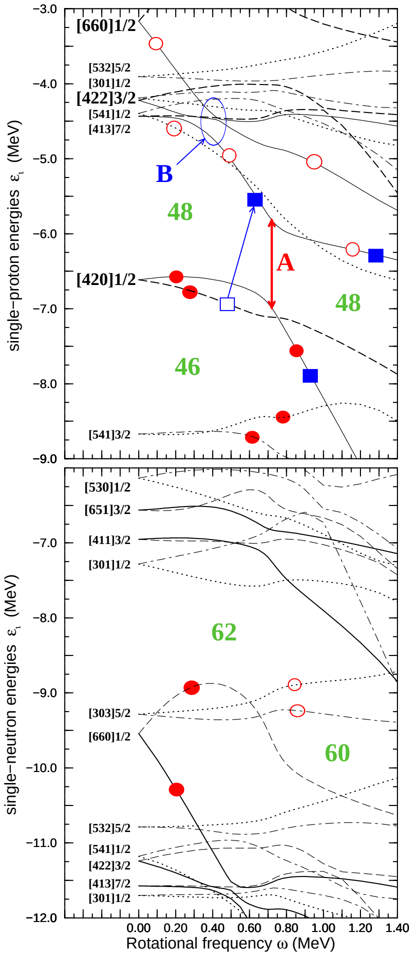

FIG. 2: Proton (top) and neutron (bottom) single-particle energies (routhians) in the self-consistent rotating potential as a function of the rotational frequency ω. They are given along the deformation path of the configuration ($\pi 6^1 \nu 6^2$ above the band crossing) assigned to the band 1. Solid, short-dashed, dot-dashed and dotted lines indicate $(\pi = +, r = -i)$, $(\pi = +, r = +i)$, $(\pi = -, r = +i)$ and $(\pi = -, r = -i)$ orbitals, respectively. At $\omega = 0.0$ MeV, the single-particle orbitals are labeled by means of the asymptotic quantum numbers $[N n_z \Lambda]\Omega$ (Nilsson quantum numbers) of the dominant component of the wave function. Large Nilsson labels are used to indicate the proton orbitals which participate in unpaired band crossings seen in the bands 1 and 2. These unpaired band crossings are indicated by the arrow A (band 1) and ellipse B (band 2). Solid (open) circles indicate the orbitals occupied (emptied) in the configuration assigned to the band 1. Solid (open) squares show the orbitals occupied (emptied) in the configuration of the band 2 as compared with the one of the band 1.

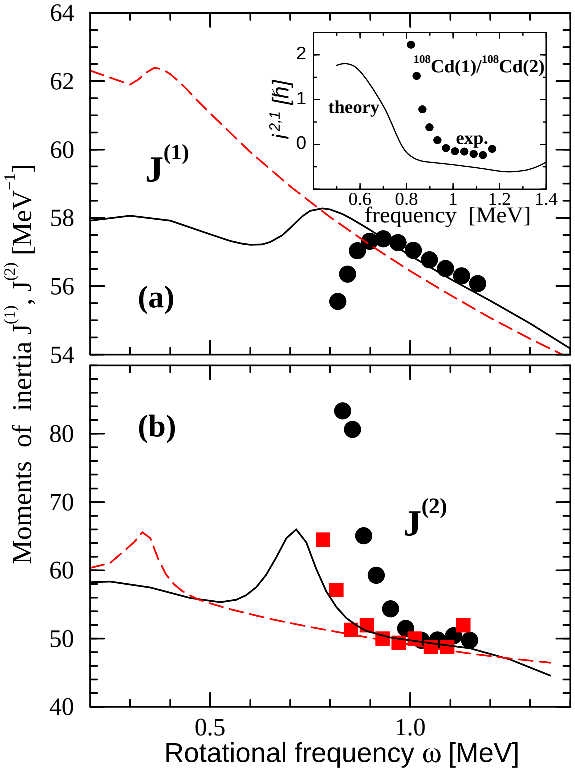

FIG. 3: Kinematic (panel (a)) and dynamic (panel (b)) moments of inertia. Circles and squares are used for the bands 1 and 2, respectively. Their theoretical counterparts are shown by solid and dashed lines, respectively. Kinematic moment of inertia of the band 1 is shown under assumption that the spin of its initial state is $I_0 = 44\hbar$. The comparison of calculated and experimental kinematic moments of inertia for band 2 as well as relative alignment analysis suggest spin $I_0 = 43\hbar$ for its lowest state. With this spin assignment $J^{(1)}$ moment of inertia of band 2 is lower by only ~ 0.2 MeV^{-1} than $J^{(1)}$ of band 1 at $\omega \geq 0.95$ MeV and, thus, for simplicity it is not shown in panel (a). The insert compares calculated and experimental (with suggested spin assignments) relative alignments of bands 2 and 1, defined as $i^{2,1}(\omega) = I_2(\omega) - I_1(\omega)$ [3].

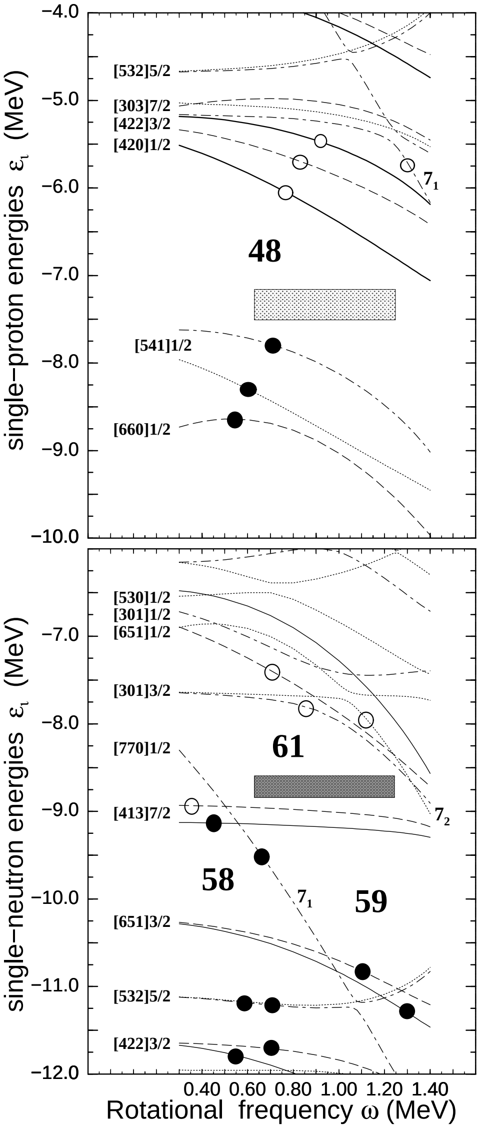

FIG. 4: The same as Fig. 2, but along the deformation path of hyperdeformed $\pi 6^2 \nu 6^4 7^1$ configuration. Dashed box indicates the frequency range corresponding to the spin range $I = 44 - 84\hbar$ in this configuration. Solid (open) circles indicate the occupied (emptied) orbitals. The labels $7_{1,2}$ are used to show two lowest $N = 7$ orbitals.

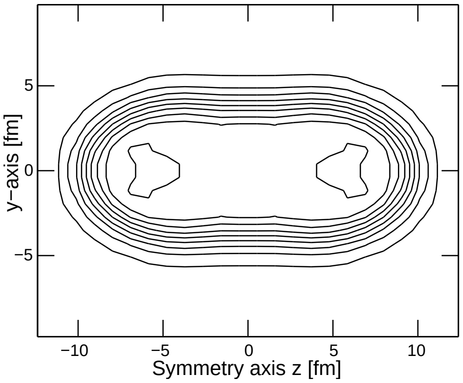

FIG. 5: The self-consistent neutron density $\rho_n(y,z)$ as a function of $y-$ and $z-$ coordinates for lowest HD configuration ($\pi 6^2 \nu 6^4 7^1$) at rotational frequency $\omega = 1.0$ MeV. The densities are shown in steps of 0.01 fm^{-3} starting from $\rho_n(y,z) = 0.005$ fm^{-3}.